Available online at www.sciencedirect.com
SCIENCE DIRECT®
Polymer 45 (2004) 3835–3843
polymer
www.elsevier.com/locate/polymer

Computer simulation studies on overlapping polymer chains confined in narrow channels

Iwao Teraoka[a,*], Yongmei Wang[b]

[a]Herman F. Mark Polymer Research Institute, Polytechnic University, Six MetroTech Center, 333 Jay Street, Brooklyn, NY 11201, USA
[b]Department of Chemistry, University of Memphis, Memphis, TN 38152-3522, USA

Received 24 February 2004; received in revised form 23 March 2004; accepted 24 March 2004

Abstract

Conformation of polymer chains strongly confined in a narrow channel space was studied over a broad range of polymer volume fractions ϕ using lattice Monte Carlo simulations. The longitudinal component of the chain dimension decreased in a power law of $\sim\phi^{-1}$ as ϕ exceeded the overlap volume fraction. The conformation changed from the one extended along the channel to a random coil. The change occurred without much overlap between adjacent chains. As the conformational transition was completed, the chains started to penetrate each other. Contraction of the chains became more gradual, and eventually the longitudinal component of the chain dimension approached that of the unconfined chains with the overall chain dimension being smaller than that of the unconfined chains. Predictions of the scaling theory were thus confirmed with additional detailed information on the state of confined chains in each regime of characteristic ϕ dependence of chain dimensions.

Keywords: Confinement; Channel; Semidilute solutions

1. Introduction

Polymer chains confined to a channel-like pore are found in many systems. Protein channels of a lipid bilayer provide such environment [1–3]. Widely used porous silica such as silica gels and controlled pore glasses [4] has pore structures that are closer to the channel geometry rather than to the slit geometry. Partitioning of polymer chains between a narrow pore and its surrounding unconfined space underlies size exclusion chromatography. Its high-concentration version that utilizes high osmotic pressure of semidilute solutions has demonstrated usefulness in separation of polymer by molecular weight [5,6] and chemical composition [7].

Thermodynamics of polymer solutions over a broad range of the concentrations, confined in a slit space or in a channel-like pore, were considered by Daoud and de Gennes using scaling theory [8]. However, their discussion about the chain conformation in the channel led to an inconsistency that the volume fraction be greater than unity. Subsequently, Brochard and de Gennes [9] corrected the mistake, but the correction was limited to molten polymers in the channel. This situation is also described in de Gennes' textbook [10]. Recently, Lal et al. [11] extended the correction to solutions.

Although the scaling theory on the confined polymer solutions was presented long ago [8], many predictions of the theories have not been confirmed or disproved in experiments or computer simulations. For instance, we do not know whether the confined chain is expanded or not, especially at high concentrations or in the melt. Experimental investigations on the state of confined polymer solutions have been plagued by a lack of model systems suitable for verification of the scaling theory and by questions on reliability of extracting the chain conformation from the experimental data. A Monte Carlo simulation study would be an appropriate method to clarify these ambiguities and test the predictions of the scaling theory.

Lattice and off-lattice Monte Carlo simulations in a channel space have been conducted, mostly for a single chain [12–15]. Contraction of confined chains with an increasing concentration was observed in the slit geometry [16–18]. The contraction was also observed in the channel geometry [19], but the confinement was not sufficiently

* Corresponding author. Tel.: +1-718-260-3466; fax: +1-718-260-3125.
E-mail address: teraoka@poly.edu (I. Teraoka).

0032-3861/$ - see front matter © 2004 Elsevier Ltd. All rights reserved.
doi:10.1016/j.polymer.2004.03.070

strong to cause the chain to adopt an extended conformation as expected at low concentrations. A thorough analysis of the chain conformation in solutions confined in the channel has not been performed.

This paper is organized as follows. The first part reviews the most recent form of the scaling theory on polymer chains confined to a pore of channel geometry in a broad range of confinement strengths and polymer volume fractions, with additional remarks of our own on the chain dimensions. After describing the procedure of lattice Monte Carlo simulations, we will present the results on the dimensions of chains strongly confined to channels over a broad range of volume fractions. The results in different regimes of volume fraction will be analyzed in the light of the scaling theory.

2. Scaling theory of polymer solutions confined in channels

We consider linear chains consisting of N monomers of size b. Properties of confined polymer solutions in channels can be well understood using the phase diagram illustrated in Fig. 1 [8]. The x axis is R_0/d, the confinement strength, where $R_0 \cong bN^{3/5}$ is the dimension of an isolated polymer chain in the bulk solution, and d is the channel width. The y axis is R_0/ξ, where ξ is the characteristic length in the bulk solution that has the same volume fraction ϕ as that of the confined solution. In dilute solutions, the characteristic length is the mean distance between nearest pair of polymer chains. In semidilute solutions, ξ is equal to the correlation length in monomer density fluctuations, $\xi \cong b\phi^{-3/4}$.

The highest possible volume fraction is $\phi = 1$ in the melt in which $\xi \cong b$. The smallest possible pore size is the monomer size b. Then, the maximum is $R_0/b \cong N^{3/5}$ for both x and y in Fig. 1. The scaling theory divides the available space of x and y into five regimes, I through V [11]. Below we review the theoretical predictions that lead to the above diagram and discuss the chain conformation in each of the regimes.

Regime I is an unconfined dilute polymer solution. Each polymer chain is a self-avoiding walk, and its dimension R is given as $R \cong R_0$. Regime II is an unconfined semidilute solution. The crossover from regime I to regime II occurs when ϕ exceeds the bulk overlap volume fraction $\phi_b^* \cong N^{-4/5}$. In regime II, we have the well-known result

$$R \cong bN^{1/2}\phi^{-1/8} \tag{1}$$

Regime III is a dilute solution confined in a narrow pore. The crossover from regime I to regime III is specified by line CC_x which is $d \cong R_0$. The latter view is an oversimplification of the real situation, as pointed out by van Vliet et al. [20]. An instantaneous conformation of a polymer chain is not spherical, but is rather

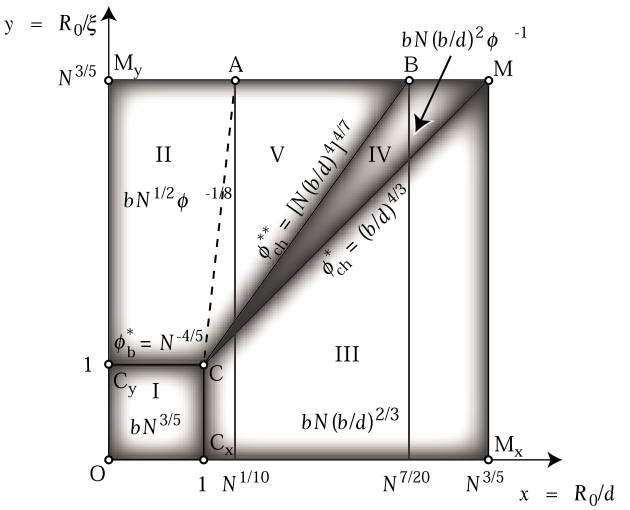

Fig. 1. Phase diagram for polymer chains consisting of N monomers of size b confined in a channel of width d. The x axis expresses the confinement strength, and the y axis gives a measure of polymer volume fraction ϕ through the characteristic length ξ. Either the overall dimension of the polymer chains or the longitudinal dimension is indicated in each of the five regimes, I through V. Volume fractions at some regime boundaries are also indicated.

approximated by an ellipsoid. The crossover region from the unconfined chain to the confined chain can be divided into a few sub-regimes: With a decreasing channel width d, the chain first aligns its longest axis along the channel axis, and then upon a further decrease in d, the chain contracts first in the direction perpendicular to the channel axis without much expansion in the parallel direction, followed by expansion in the parallel direction. As a general rule, the crossover from I to III occurs at around $x = R_0/d = 0.5$ [20]. However, we will adopt here the simpler view mentioned at the beginning of this paragraph.

In regime III, each isolated chain in a narrow channel adopts a plug-like conformation extending along the channel, which Daoud and de Gennes called a cigar [8]. The polymer chain is a train of spheres of diameter d, and, within each sphere, the partial chain adopts the conformation of an excluded-volume chain. Therefore, longitudinal dimension of the chain is given as

$$R_{\|0} \cong bN(b/d)^{2/3} \tag{2}$$

We use $\|$ and $\perp$ in the subscript to denote the chain dimension in the directions parallel and perpendicular, respectively, to the channel axis. One-dimensional nature is evident in the relationship of $R_{\|0} \sim N$.

The crossover from the dilute solution of one-dimensional cigars (regime III) to a semidilute solution of touching cigars (regime IV) occurs at the overlap volume fraction in the channel, $\phi_{ch}^* \cong Nb^3/(R_{\|0}d^2)$, which yields

$$\phi_{ch}^* \cong (b/d)^{4/3} \tag{3}$$

Note that ϕ_{ch}^* is independent of N. Eq. (3) gives line CM,

$x \cong y$, in Fig. 1. One can find that, on CM, ξ in the bulk solution of the same ϕ is equal to d. As soon as the cigars begin to touch each other, ξ is already smaller than d. Therefore, in a confined semidilute solution in the channel, there is only one isotropic correlation length. In the slit, in contrast, the correlation length is different between the directions parallel and perpendicular to the slit walls when confined chains start to overlap within the slit.

Now we consider narrowing the channel in regime II. The onset of confinement with a decreasing d is somewhat delayed at higher polymer volume fractions. Dashed line CA demarcates regime II from regime V in which the overlapping chains experience the confinement effect. Line CA is not vertical, since the chain contraction at higher volume fractions eases the confinement strength. The line, given by $y \cong x^6$, is determined by $d \cong R$, where R is given by Eq. (1). At point A, $x \cong R_0/(bN^{1/2}) \cong N^{1/10}$ or $d \cong bN^{1/2}$.

There is another crossover line CB, which was absent in the first discussion by Daoud and de Gennes [8]. The presence of point B on line M_yM was pointed out by Brochard and de Gennes [9]. It was explained as follows: On line M_yM, $\xi \cong b$. At M_y, one has a three-dimensional melt, therefore $R \cong bN^{1/2}$. At M, in contrast, the chain is fully extended in the channel of width $d \cong b$, and therefore $R \cong bN$. The difference between these two expressions of R is also manifested by the difference in the internal filling volume fraction, ϕ_{int}, which is the volume fraction of the monomers on a given chain over the volume subtended by the chain. At M_y, $\phi_{\text{int}} \cong Nb^3/(bN^{1/2})^3 \cong N^{-1/2} < 1$, whereas at M, $\phi_{\text{int}} \cong 1$. The chains penetrate each other to bring the total volume fraction to unity at M_y, but the chain cannot penetrate each other at M. They can only be packed tightly head-on. The crossover point B does not coincide with A; At A, ϕ_{int} is still around $N^{-1/2}$.

At B, the confined chain in the channel has $R_\| \cong bN^{1/2}$ and $R_\perp = d$. Then, by requiring $\phi_{\text{int}} = Nb^3/(R_\| d^2) \cong 1$, one finds that $d \cong bN^{1/4}$ gives B. Therefore, $x \cong N^{7/20}$ at B. Between A and B, $R_\|$ is held unchanged at $bN^{1/2}$. If this $R_\|$ continues between B and M, then $\phi_{\text{int}} > 1$, an impossible situation. Therefore, on line BM, the longitudinal dimension of the chain will be perturbed. Chains will start to segregate and expand in its longitudinal dimension as $R_\| \cong Nb^3/d^2$ to maintain $\phi_{\text{int}} \cong 1$.

The above discussion can be extended to solutions [11]. Line CB divides the semidilute confined solutions into two regimes: regime IV in which cigars touch each other but do not penetrate, and regime V in which cigars penetrate each other. In regime V, $R_\| \cong bN^{1/2}\phi^{-1/8}$ and $R_\perp \cong d$. The crossover volume fraction on line CB, ϕ^{**}_{ch}, can be found by requiring $\phi_{\text{int}} \cong Nb^3/(d^2 R_\|) \cong \phi$, with $R_\|$ given just above, which leads to

$$\phi^{**}_{\text{ch}} \cong [N(b/d)^4]^{4/7} \tag{4}$$

or $y = x^{12/7}$ for line CB.

The chain contraction in regime IV is found by requiring that the chains do not penetrate

$$R_\|/R_{\|0} \cong (\phi/\phi^*_{\text{ch}})^{-1} \tag{5}$$

where $R_{\|0}$ is given by Eq. (2). The same relationship can be found using the scaling function. The chain dimension $R^{**}_\|$ at ϕ^{**}_{ch} can be readily obtained, using Eqs. (4) and (5), as

$$R^{**}_\|/R_{\|0} \cong (\phi^{**}_{\text{ch}}/\phi^*_{\text{ch}})^{-1} \cong (N^{3/5}b/d)^{-20/21} \cong (R_0/d)^{-20/21} \tag{6}$$

A summary of the chain dimensions in the five regimes and the crossover volume fractions is given in Fig. 1. The dimension is R when unconfined (I, II), and $R_\|$ when confined (III, IV, V).

Increasing the polymer volume fraction in a channel of a given width amounts to moving a point along a relevant vertical line in Fig. 1. One readily notices that, unless the channel is extremely narrow, the confined solution will undergo a crossover from regime III to IV, and then into V. Only when the channel is extremely narrow, the solution will not enter regime V.

The diagram can be used to predict the equilibrium of a solution of polymer chains between a narrow channel and the unconfined space [8]. At sufficiently low concentrations in the solution exterior to the channel, the chains find it difficult to enter the channel. With an increasing concentration, ξ decreases in the exterior. When ξ becomes smaller than d, polymer chains will rush into the channel (weak-to-strong penetration transition).

We now compare $R_\|$ of polymer chains in the channel, slit, and bulk. We assume that the chains are strongly confined in the channel or in the slit, but $d > bN^{1/4}$. In the slit, $R_\|$ is the chain dimension in the direction parallel to the slit walls. In the bulk, $R_\|$ is taken in any direction. Fig. 2 is a schematic drawing of $R_\|$, reduced by b, as a function of ϕ in a double logarithmic scale for the chains in the three spaces.

In the slit, as ϕ exceeds $\phi^*_{\text{sl}} \cong (b/dN)^{1/2}$ [9], higher than $\phi^*_b \cong N^{-4/5}$, chains contract as two-dimensional chains until ϕ reaches ϕ^{**}_{sl} when the longitudinal correlation length becomes comparable to d. Beyond ϕ^{**}_{sl}, $R_\|$ decreases as in the bulk. It is interesting to see that $\phi^{**}_{\text{sl}} \cong \phi^*_{\text{ch}}$; polymer chains in the channel do not feel the presence of other chains until such a high volume fraction is reached. The channel extends the polymer chains most and delays the onset of the contraction most. The rate of contraction is greater in the slit than it is in the bulk, and even more so in the channel to catch up with a slowly decreasing bulk dimension.

3. Simulation procedure

Monte Carlo simulations were conducted for self-avoiding walks on a cubic lattice. Monomers (beads) of polymer chains can occupy lattice sites in a box of $L_x \times L_y \times L_z$ in x, y, and z directions with $L_x = L_y$ and $L_z = 4096$, where the unit length is a lattice spacing ($b = 1$). Four walls are at $x = 0$ and $L_x + 1, y = 0$ and $L_x + 1$. A periodic

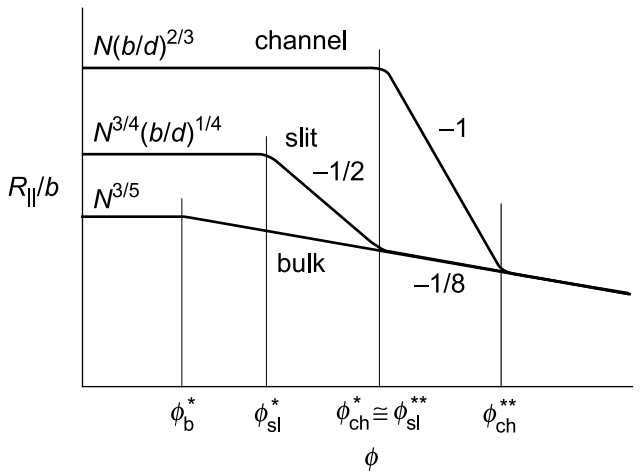

Fig. 2. Linear dimension of chains consisting of N monomers confined in a channel and a slit of width d and the dimension of the same chains in bulk solutions are schematically compared. The scales of both axes are logarithmic. The characteristic slope of the power law in each section is indicated adjacent to the plot.

boundary condition applies to the z direction. The channel width is $d = L_x + 1$. No interactions were assumed for the beads except for no occupancy at already filled sites or at walls. Polymer chains consisting of N beads with $N = 1000$ and 2000 were generated in either a straight or a random-coil conformation and moved according to Metropolis rule [21] and reptation. It was decided that the system had reached an equilibrium when the ensemble average of the radius of gyration exhibited no discernible decreasing or increasing trend over 10^8 trial moves per chain. The box size used in the present study is $L_x = 11$, 13, and 17 for $N = 1000$ and $L_x = 17$ for $N = 2000$. The ratio of R_{g0} to d is often used to express the confinement strength for a single chain, where R_{g0} is root-mean-square radius of gyration in unconfined space. The values of R_{g0}/d are 5.30, 4.54, 3.53 in channels of $L_x = 11$, 13, and 17, respectively, for $N = 1000$, and 5.32 in the channel of $L_x = 17$ for $N = 2000$.

To characterize the anisotropic chain dimensions, four quantities were calculated: $R^2_{\|}$ and $R^2_{\perp}$, the z and x-components of the mean square end-to-end distance; $R^2_{g\|}$ and $R^2_{g\perp}$, the z and x-components of the mean square radius of gyration. The x-components are actually the mean of the x and y-components of the respective dimensions. We use $R_{\|}, R_{\perp}, R_{g\|}$, and $R_{g\perp}$ to denote their root mean squares. For the rest of the paper, $R_{\|}$ and $R_{\perp}$ mean the end-to-end distances, not just anisotropic chain dimensions in general as used in Section 2.

Sampling of chain dimensions started after equilibration. The four averages were calculated over the chains in the ensemble every 10^6 trial moves, and then their long-time averages were calculated. The number of trial moves needed for reliable averages were 9×10^9 for a single chain of $N = 1000$ in $L_x = 17$ to 3.8×10^{11} for 200 chains of $N = 2000$ in $L_x = 17$. Two runs of simulation were conducted for $N = 2000$ in $L_x = 17$, starting from different initial configurations at each of 16 different volume fractions. The relative difference of $R_{\|}$ or $R_{g\|}$ between the two runs was less than 1%. In some of the figures in the present paper, two symbols are shown at each of these ϕ, but they are hardly distinguishable. The relative difference in $R_{\perp}$ or $R_{g\perp}$ between the two runs was less than 0.1%.

For reference purposes only, we also performed lattice simulations for single chains of different lengths ($N = 100$, 200, 500, 1000, 2000, 4000, 7000, and 10000) in channels of different widths ($L_x = 6$ to 19 for $N = 100$, $L_x = 7$ to 70 for $N = 10000$). Their root-mean-square end-to-end distances R_0 in unconfined space and R_{g0} are listed in Table 1. The purpose of this part of simulation is to obtain $R^2_{\|0}/R^2_{g\|0}$ under various confinement strengths, where $R_{\|0}$ and $R_{g\|0}$ are the values of $R_{\|}$ and $R_{g\|}$, respectively, of a confined single chain.

4. Results and discussions

Fig. 3 shows changes in $R_{\|}, R_{g\|}, R_{\perp}$, and $R_{g\perp}$ with ϕ for $N = 2000, L_x = 17$. The pattern is similar for the other three combinations of N and L_x studied here. The change in the longitudinal dimension of the chain clearly gives three regimes that are identified as regimes III through V. In regime III, all of the four dimensions remain unchanged. In regime IV, the two longitudinal dimensions decrease steeply as ϕ^{-1} and gradually in regime V. We find that $d > bN^{1/4}$ for all of the four systems, hence we expect to see a crossover from regime IV to regime V according to the diagram in Fig. 1.

The conformation of polymer chains remains highly anisotropic in the entire range of volume fractions. For $N = 2000, L_x = 17, R_{g\|}/R_{g\perp}$ decreases from 18.4 to 4.00. For $N = 1000, L_x = 17$, the weakest confinement in the present study, $R_{g\|}/R_{g\perp}$ decreases from 9.23 to 2.87. The dependence of $R_{\|}$ on N, although only two chain lengths were examined in the present study, also agrees with the scaling predictions. The ratio of $R_{\|}$ for $N = 2000$ to $R_{\|}$ for $N = 1000$ in the channel of $L_x = 17$ is 2.1 in regime III and 1.5 in regime V. The latter ratio agrees with $R_{\|} \sim N^{1/2}$.

Bird's-eye view of snapshots of chains are shown in Fig. 4 for chains of $N = 2000$ in the channel of $L_x = 17$. In

Table 1
Dimensions of single chains in unconfined space

N	R_0	R_{g0}	R^2_0/R^2_{g0}
100	16.17	6.428	6.325
200	24.56	9.763	6.327
500	42.29	16.86	6.294
1000	63.61	25.37	6.285
2000	95.81	38.24	6.277
4000	144.0	57.53	6.266
7000	201.2	80.29	6.280
10,000	248.2	99.04	6.281

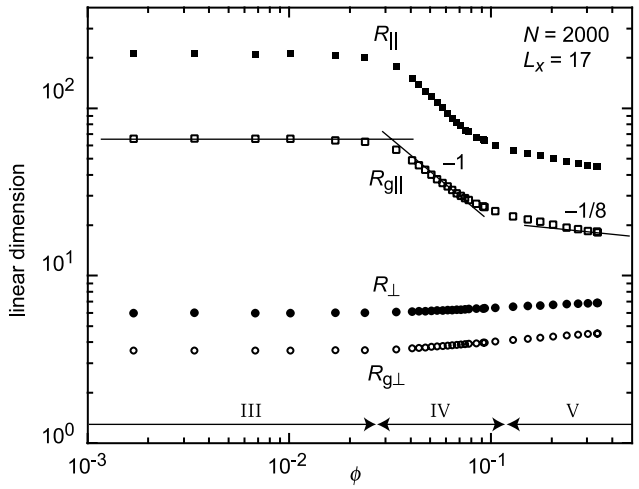

Fig. 3. Longitudinal and lateral chain dimensions, $R_{\|}$ (closed squares), $R_{g\|}$ (open squares), $R_{\perp}$ (closed circles) and $R_{g\perp}$ (open circles), plotted as a function of polymer volume fraction ϕ, for $N = 2000, L_x = 17$. Three lines have a slope of 0, −1, and −1/8. Three regimes of ϕ, III through V, are indicated above the bottom axis.

part a ($\phi = 0.00676$, regime III), the chains are isolated from each other. In part b ($\phi = 0.0473$, regime IV), the chains are bumped against their neighboring chains without much overlap. Some are overlapped with neighbors, but the overlapped section is just a small part of the space occupied by a chain. There are no square cross sections that have beads from three chains. Congestion is heavier in part c ($\phi = 0.1521$, regime V). Most of the chains are still not much overlapped with neighbors, but some are intertwined with other chains. With a further increase in ϕ, the chains become highly intertwined in part d ($\phi = 0.3379$, regime V), in accordance with the prediction of the scaling theory.

Fig. 5 shows the fraction $f_i (i = 1, 2, \ldots)$ of square cross sections in the channel that have beads from i chains. The figure is for $N = 2000$ in $L_x = 17$. Empty cross sections were excluded from the tally. The fractions were calculated from a single shot of chain configurations, and therefore the symbols are not on smooth curves. The four volume fractions in Figs. 4a–d are indicated by the arrows. In regime III, $f_1 = 1$ and $f_i = 0$ for $i = 2, 3, \ldots$ All cross sections contain only beads from one chain, if they have beads. At around ϕ^*_{ch}, f_2 starts to increase, but f_3 remains zero in regime IV. As the system enters regime V, f_3 starts to rise, followed by f_4 at higher volume fractions. Even at the highest ϕ, f_i is non-zero only up to $i = 6$.

To examine the crossover from regime III to IV, $R_{\|}/R_{\|0}$ is plotted in Fig. 6 as a function of ϕ/ϕ^*_{ch} for all combinations of N and L_x studied. Here, ϕ^*_{ch} was estimated from $\phi^*_{ch} = Nb^3/(R_{\|0}L_x^2)$, where the value of $R_{\|0}$ determined from the simulation for a single chain was used. As ϕ/ϕ^*_{ch} approaches one, all the data start to decrease along a common straight line with a slope close to −1, in agreement with Eq. (5). The data deviate upward at higher volume fractions, as the system enters regime V. The deviation occurs at a different ϕ/ϕ^*_{ch} for each combination of N and L_x, since the dependence of ϕ^{**}_{ch} on N and d are different from the one for ϕ^*_{ch}. For strongly confined chains, especially for $N = 1000$ in channels of $L_x = 13$ and $N = 2000$ in $L_x = 17$, the slope in regime IV is slightly more negative. We also prepared a plot of $R_{g\|}/R_{g\|0}$ as a function of ϕ/ϕ^*_{ch} for all combinations of N and L_x studied (not shown). The data follow a single master curve in regimes III and IV. The slope in regime IV is slightly more gradual than −1. The difference between the two parts is related to the ratio of $R_{\|}$ and $R_{g\|}$, which is examined below.

The nature of chain conformation can also be seen in the plot of $R^2_{\|}/R^2_{g\|}$. In regime III, the beads of a confined chain occupy a rectangular space with a uniform density

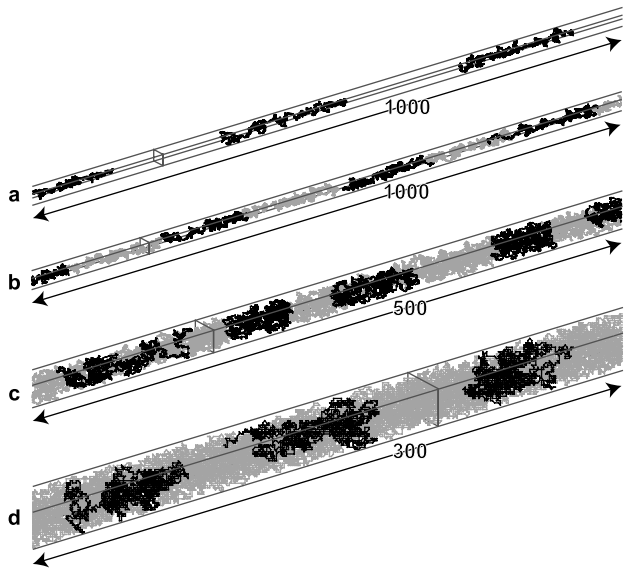

Fig. 4. Snapshot of chain conformations for chains of $N = 2000, L_x = 17$ at four polymer volume fractions: (a) 0.00676, (b) 0.0473, (c) 0.152, and (d) 0.338. Some chains are drawn in black; others in gray. The numbers on straight lines with arrows on the ends indicate the longitudinal lengths of the channel section displayed. A square cross section is drawn in each part.

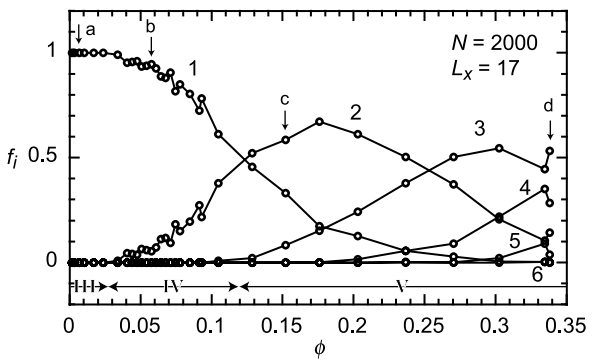

Fig. 5. Fraction $f_i (i = 1, 2, \ldots)$ of square cross sections in a channel of $L_x = 17$ that have beads from i chains of $N = 2000$. The i is indicated adjacent to each curve. The arrows with 'a' through 'd' point to the four conformations in Fig. 4. Three regimes of ϕ, III through V, are also indicated.

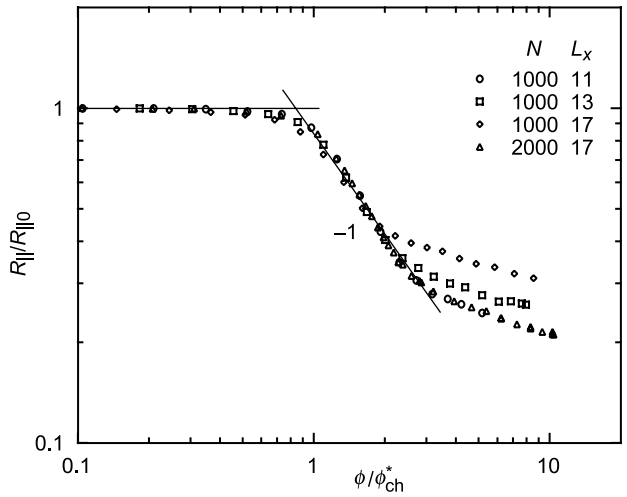

Fig. 6. Root mean square of the end-to-end distance along the channel axis reduced by its value for a single chain, plotted as a function of reduced volume fraction, ϕ/ϕ^*_{ch}. The legend shows N and L_x. Two lines have a slope of 0 and -1.

along the channel axis [8,10]. It then appears natural to expect that $R^2_{\|}/R^2_{g\|}$ is equal to 12 for a completely extended chain in a sufficiently narrow pore. In unconfined space, in contrast, the ratio is 6 if it is an ideal chain, and 6.30 for an excluded-volume chain [22].

Before examining $R^2_{\|}/R^2_{g\|}$ for confined chains at different volume fractions, we first look at the ratio for single chains of different lengths in channels of different widths. Fig. 7 presents $R^2_{\|0}/R^2_{g\|0}$ for these chains. All the points are along a smooth master curve (not drawn). As the confinement strength $R_{g\|0}/d$ increases, the ratio monotonically increases from ~6.4 to 11.9. The change from a three-dimensional random coil to a one-dimensional rod is evident in the figure. We notice that an extremely strong confinement is required ($R_{g\|0}/d \cong 100$) in order for the ratio to be close to 12. At $R_{g\|0}/d = 3$, for instance, $R^2_{\|0}/R^2_{g\|0} \cong 10$, and therefore $R_{\|0}/d \cong 9.5$. It may appear that this $R_{\|0}/d$ is sufficiently large, but the confined chains are not fully extended.

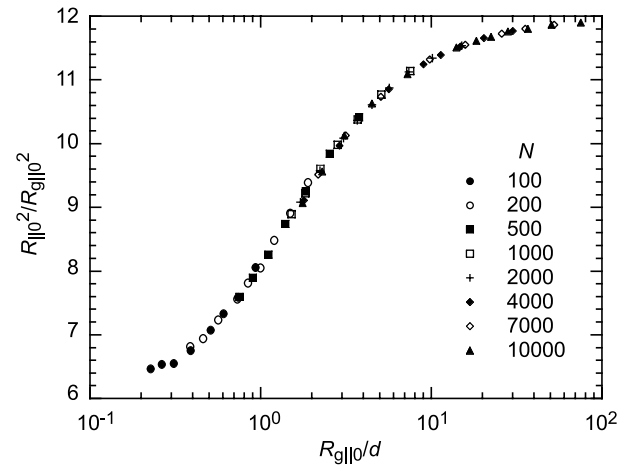

Fig. 7. The ratio of the mean square end-to-end distance to the mean square radius of gyration (longitudinal components) of a single chain in the channel, plotted as a function of $R_{g\|0}/d$. The legend shows the chain length N.

Fig. 8 shows the change in the ratio $R^2_{\|}/R^2_{g\|}$ as ϕ increases for $N = 2000, L_x = 17$ and $N = 1000, L_x = 17$. The ratio at low concentrations is substantially smaller than 12, because the confinement is not too strong, especially for $N = 1000, L_x = 17$. The ratio is steady in regime III, but sharply drops to a value close to 6 in regime IV, where cigars begin to touch each other and squeeze against each other. Although the cigars are not penetrating each other in regime IV, the squeezing from both ends effectively changes the chain conformation from an elongated rod to a random coil that just fits in a narrow channel. It is also interesting to note that the ratio is held unchanged at around 6.2 in regime V. From Fig. 8, we can conclude that the change of the chain conformation from a rod to a random coil is complete in regime IV in which the longitudinal dimension decreases as ϕ^{-1}.

How about a plot of $R^2_{\|}/R^2_{g\|}$ as a function of $R_{g\|}/d$? If $R_{g\|}/d$ determines the conformation of the chain as it does in dilute solutions, then the plot for different combinations of N and L_x will be on the same master curve as the one depicted in Fig. 7. Fig. 9 shows that it is not the case. The decrease in $R^2_{\|}/R^2_{g\|}$ with a decreasing $R_{g\|}/d$, which was caused by an increasing ϕ, is sharper than it is in Fig. 7. With an increasing confinement strength, the drop shifts to a greater $R_{g\|}/d$, that is, the shift occurs when the chains are more anisotropic. Here we see a difference in chain statistics between polymer chains with its excluded volume fully at work and polymer chains with excluded volume shielded. When chains are congested in regimes IV and V, their conformation is still anisotropic. Nevertheless, the shielding randomizes the chain conformation. For isolated chains, in contrast, randomness requires that the confinement be weak.

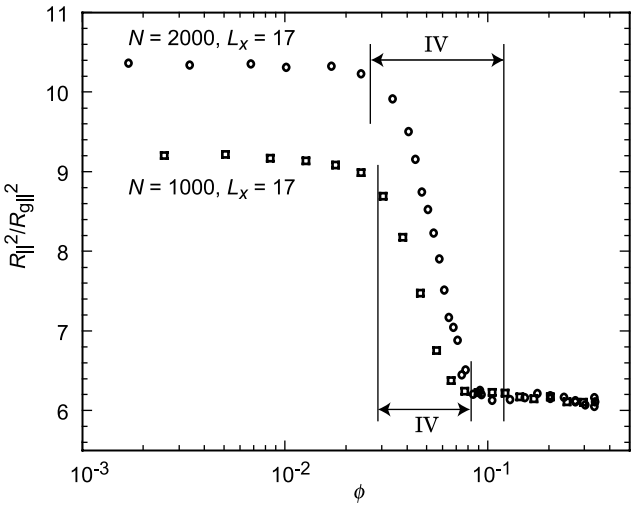

Fig. 8. The ratio of the mean square end-to-end distance to the mean square radius of gyration (longitudinal components), plotted as a function of ϕ. The upper plot is for $N = 2000, L_x = 17$, and the lower for $N = 1000, L_x = 17$. The arrows indicate regime IV for the two systems.

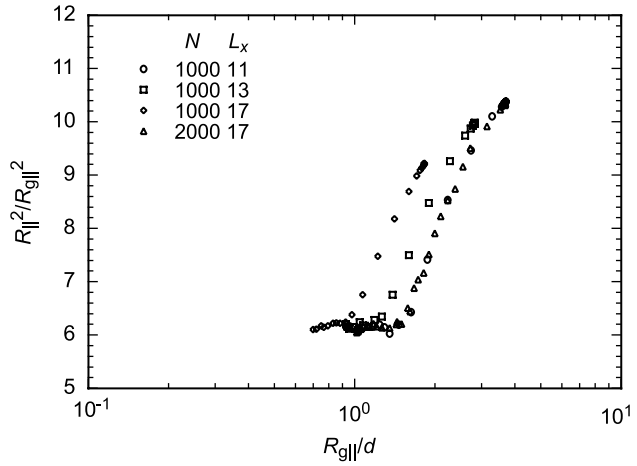

Fig. 9. The ratio of the mean square end-to-end distance to the mean square radius of gyration (longitudinal components), plotted as a function of $R_{g\|}/d$. The legend shows N and L_x. The change in $R_{g\|}$ is caused by chain contraction with an increasing polymer volume fraction.

The crossover from regime IV to V is examined here in another master plot. Translating Eq. (4) into the lattice space, we estimate ϕ_{ch}^{**} from $\phi_{ch}^{**} = [N(b/L_x)^4]^{4/7}$. Applying Eq. (6), we have $R_{g\|}^{**}$ as $R_{g\|}^{**} \cong R_{g\|0}(R_{g0}/d)^{-20/21}$. In Fig. 10, $R_{g\|}/R_{g\|}^{**}$ thus calculated for different N and L_x is plotted as a function of ϕ/ϕ_{ch}^{**}. All the data in $\phi/\phi_{ch}^{**} > 0.4$ lie along a single master curve (not drawn). The master curve has a slope close to -1 at $\phi/\phi_{ch}^{**} < 0.6$, and above that range the slope changes gradually to about $-1/8$. The change is, however, surprisingly slow. Because of the limited range of confinement strength R_{g0}/d in the present study, we cannot tell whether the transition will become more distinct with an increasing R_{g0}/d.

We now compare the chain dimension in the confined solution with that in the bulk solution. Part a of Fig. 11 compares $R_{g\|}$ for $N = 1000$ in $L_x = 11$, 13, and 17 with $3^{-1/2}$

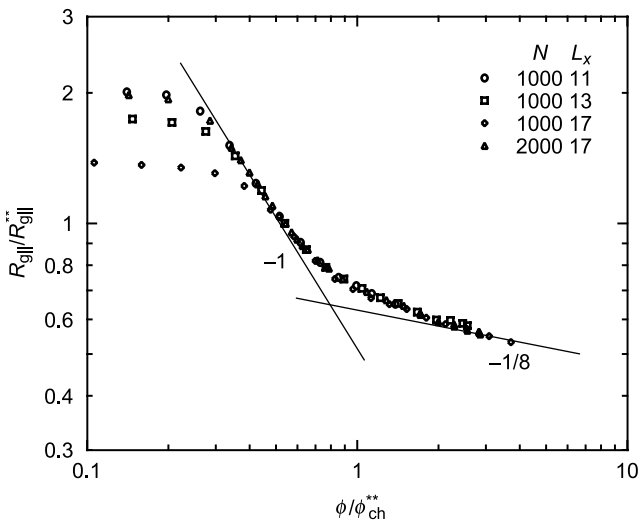

Fig. 10. Root mean square radius of gyration along the channel axis reduced by $R_{g\|}^{**}$, plotted as a function of reduced volume fraction, ϕ/ϕ_{ch}^{**}. The legend shows N and L_x. Two lines have a slope of -1 and $-1/8$.

of the radius of gyration R_g in the bulk solution of the same ϕ (solid line). The R_g in the bulk solution was calculated using the empirical chain contraction formula obtained earlier in the simulation study [17]. In the absence of confinement or if the confinement is weak, $R_{g\|}$ would be identical to the solid line. The figure also shows $R_{g\perp}$, which would be identical to the solid line were it not for the confinement. Part b of Fig. 11 compares the overall R_g, where $R_g^2 = R_{g\|}^2 + 2R_{g\perp}^2$, with the radius of gyration in the bulk solution of the same ϕ (solid line).

In regimes III and IV, the plots of $R_{g\|}$ are located much higher than the solid line is. They approach the solid line in regime V, but there is still a gap. In contrast, $R_{g\perp}$ is smaller than $3^{-1/2}$ of the bulk R_g, since $R_{g\perp} < d$ in the confined solution. The overall R_g in the confined solution is larger than it is in the bulk solution in dilute solutions, but becomes smaller than the bulk value with an increasing ϕ when $R_{g\|}$ drops rapidly in regime IV. Although there is a difference in the magnitude between the radii of gyration of chains in the two spaces, the results in Fig. 11 agree with the schematic drawing in Fig. 2. Similar results were observed for the solutions confined to a slit [17]. Experimental studies by Lal et al. also confirmed this phenomenon [20].

Our results on confined solutions can be extrapolated to a melt confined in the channel. As long as the channel is not so narrow as to bring the melt onto line BM in Fig. 1, the

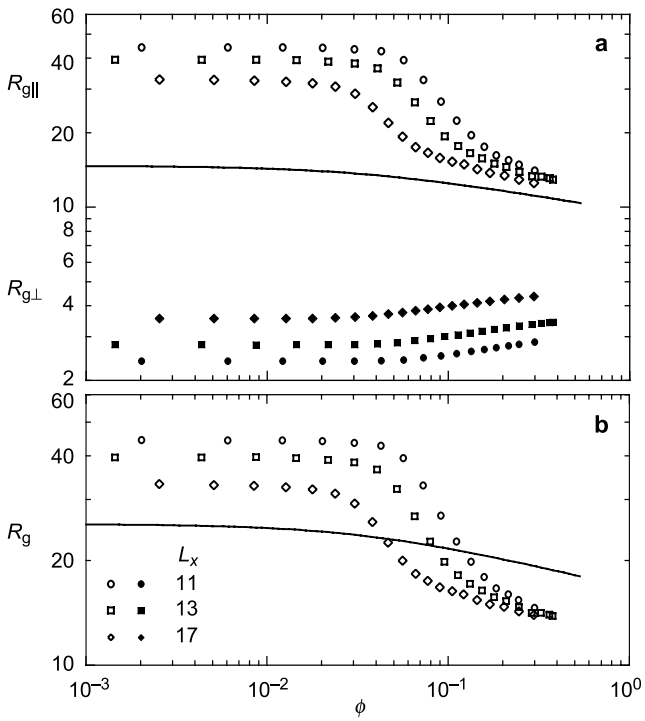

Fig. 11. (a) Root-mean-square longitudinal ($R_{g\|}$, open symbols) and lateral ($R_{g\perp}$, closed symbols) components of radius of gyration for chains of length $N = 1000$ confined to a channel of wall-to-wall distance $b(1 + L_x)$, plotted as a function of the polymer volume fraction ϕ. The solid line is $3^{-1/2}$ of the radius of gyration in unconfined solution. (b) Overall radius of gyration of confined chains. The legend shows L_x. The solid line indicates the radius of gyration in unconfined solution.

overall dimension of chains confined to the channel will be smaller compared with the one in the unconfined melt. The chain is highly anisotropic, however, with the longitudinal dimension maybe comparable with the bulk value, and the lateral dimension close to the channel width.

Finally we take a look at $R_\perp$ and $R_{g\perp}$. Figs. 3 and 11 have already shown that $R_\perp$ and $R_{g\perp}$ increase as ϕ increases. Fig. 12 shows $R_\perp/d$ and $R_{g\perp}/d$ for all combinations of N and L_x of the present simulation studies as a function of ϕ/ϕ^*_{ch}. In each of $R_\perp/d$ and $R_{g\perp}/d$, all the data collapse onto a single master curve, except the data of $R_{g\perp}/d$ for $N = 1000, L_x = 17$ at high volume fractions. The slight downward deviation for $N = 1000, L_x = 17$ is ascribed to a weak confinement at these high volume fractions.

In contrast to $R_\parallel$ and $R_{g\parallel}$ that have three regimes of volume fraction dependence, $R_\perp/d$ and $R_{g\perp}/d$ have only two regimes separated by ϕ^*_{ch}. At low volume fractions (regime III), the collapse is a signature of strong confinement: $R_\perp/d$ and $R_{g\perp}/d$ are not being affected by N or d. The ratio remains constant in this regime ($R_\perp \cong d, R_{g\perp} \cong d$), consistent with the scaling theory predictions. At $\phi > \phi^*_{ch}$, the chains continue to expand laterally, and the expansion is again independent of N. These behaviors can be explained as follows. At $\phi < \phi^*_{ch}$, the monomer density profile across the channel of $0 < x < d$ and $0 < y < d$ is close to $\sin^2(\pi x/d)\sin^2(\pi y/d)$ [19]. Therefore, $R_\perp/d$ and $R_{g\perp}/d$ are independent of N or d. At $\phi > \phi^*_{ch}$, the correlation length ξ is smaller than d and continues to decrease as ϕ increases. When $\xi \ll d$, the density profile is flat in the center and drops to zero toward the walls. The thickness of the depletion layer at the walls is $\sim\xi$. This is why $R_\perp$ and $R_{g\perp}$ increase in regimes IV and V. The master curve (not drawn) in Fig. 12 indicates that ξ/d is not a function of N, but depends on ϕ/ϕ^*_{ch} only in the whole range of ϕ. The only visible regime boundary is $\phi^*_{ch} : \phi^{**}_{ch}$ applies to the longitudinal direction only.

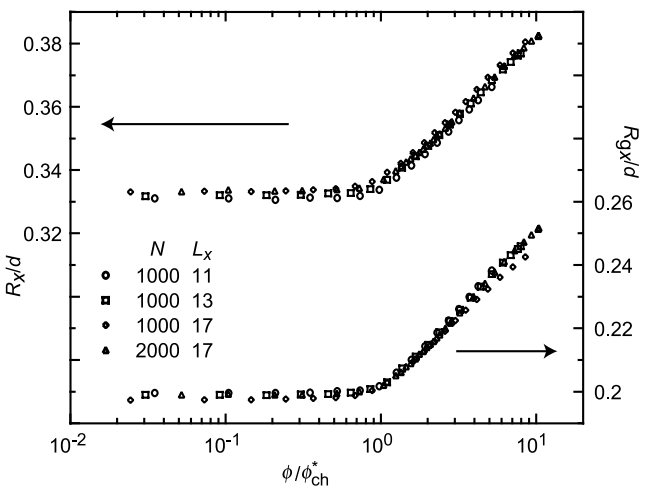

Fig. 12. Reduced lateral chain dimensions, $R_\perp/d$ and $R_{g\perp}/d$, plotted as a function of reduced volume fraction, ϕ/ϕ^*_{ch}. The legend shows N and L_x.

Simple calculation gives $R_\perp$ and $R_{g\perp}$ of ideal chains in a strong confinement: $R_\perp/d = (1/2 - (4/\pi^2))^{1/2} \cong 0.308$, $R_{g\perp}/d = (1/12 - (1/2\pi^2))^{1/2} \cong 0.181$. In the limit of the weak confinement, the numbers are to $6^{-1/2} \cong 0.408$ and $12^{-1/2} \cong 0.289$, respectively. In the melt, $\xi \cong b$, and therefore $R_\perp/d$ and $R_{g\perp}/d$ should be close to those in the weak confinement. Fig. 12 indicates that excluded-volume chains at low volume fractions exhibit larger values of $R_\perp/d$ and $R_{g\perp}/d$ than those for the ideal chains. With an increasing ϕ, $R_\perp/d$ and $R_{g\perp}/d$ approach those expected for the weak confinement in the channel. As we did for the longitudinal dimensions, we plotted $R^2_\perp/R^2_{g\perp}$ (not shown). The ratio is around 2.8 at low volume fractions, close to 2.90, the value of ideal chains, and decreases to 2.3 at the highest ϕ studied. As for the longitudinal counterpart, the ratio is insensitive to the excluded volume.

5. Conclusions

The present lattice Monte Carlo simulation study shows how polymer chains strongly confined to narrow channels contract upon increasing concentration beyond the chain overlap. We have observed the chain contraction typical of one-dimensional semidilute solutions, namely $R_\parallel \sim \phi^{-1}$, in regime IV and then a crossover to the contraction typical of three-dimensional semidilute bulk solutions, namely, $R_\parallel \sim \phi^{-1/8}$, in regime V. In regime IV, the chain conformation changes from that of a cigar to that of a random coil. The chain in regime V is still anisotropic, but the chain statistics along the longitudinal direction is similar to that of an ideal chain in which the excluded volume interaction is screened. It was also in regime IV that the overall dimension of the confined chains becomes smaller than the bulk value with an increasing ϕ. A visual verification of 'touching cigars' to 'intertwined cigars' was also presented. Our results agree with the predictions of the scaling theory.

References

[1] Bezrukov SM, Vodyanoy I, Brutyan RA, Kasianowicz JJ. Macromolecules 1996;29:8517.
[2] Kasianowicz JJ, Brandin E, Branton D, Deamer DW. Proc Natl Acad Sci USA 1996;93:13770.
[3] Movileanu L, Bayley H. Proc Natl Acad Sci USA 2001;98:10137.
[4] Haller W. Nature 1965;206:693.
[5] Luo M, Teraoka I. Macromolecules 1996;29:4226.
[6] Xu Y, Teraoka I, Senak L, Wu C-S. Polymer 1999;40:7359.
[7] Lee D, Teraoka I, Fujiwara T, Kimura Y. J Chromatogr A 2002;966:41.
[8] Daoud M, de Gennes PG. J Phys (Paris) 1977;38:85.
[9] Brochard F, de Gennes PG. J Phys (Paris) 1979;40:L399.
[10] de Gennes PG. Scaling concepts in polymer physics. Ithaca, NY: Cornell University Press; 1979.
[11] Lal J, Sinha S, Auvray LJ. J Phys II (France) 1997;7:1597.
[12] Kremer K, Binder K. J Chem Phys 1984;81:6381.
[13] van Giessen AE, Szleifer I. J Chem Phys 1995;102:9069.

[14] Sotta P, Lesne A, Victor JM. J Chem Phys 2000;112:1565.
[15] Sheng YJ, Wang MC. J Chem Phys 2001;114:4724.
[16] Wang Y, Teraoka I. Macromolecules 2000;33:3478.
[17] Teraoka I, Wang Y. Macromolecules 2000;33:6901.
[18] Cifra P, Bleha T. Makromol Chem Theor Simul 2000;9:555.
[19] Cifra P, Teraoka I. Polymer 2002;43:2409.
[20] van Vliet JH, Luyten MC, ten Brinke G. Macromolecules 1992;25:3802.
[21] Metropolis N, Rosenbluth W, Rosenbluth MN, Teller AH, Teller E. J Chem Phys 1953;21:1087.
[22] des Cloizeaux J, Jannink G. Polymers in solution: their modelling and structure. Oxford: Oxford University Press; 1989.